Geospatial Energy and Life Cycle Assessment of Oscillating Water Column Systems in the Northeast

Alexander E. Siemenn[1] and Marie-Odile Fortier[2]

[1]Department of Atmospheric and Environmental Sciences, Department of Mathematics, University at Albany, State University of New York, Albany, NY 12222, USA
[2]Department of Civil and Environmental Engineering, University of California, Merced, CA 95343, USA

(May 15, 2019)

1 Introduction

The expansion of renewable energy promotes an interest in developing technologies that harness the power stored in the ocean. One form of ocean energy harvesting technology is the Oscillating Water Column (OWC) which converts the potential energy of the oscillatory wave plane into electrical energy. Such a conversion is achieved by encapsulating the wave height oscillations in a semi-submerged, rigid concrete chamber which induces pressure changes within the chamber, respective to the wave height [2]; [3]. A duct is installed above the sea level to allow airflow in and out of the chamber as the internal pressure decreases and increases, respectively [23]. The induced airflow forces the rotation of a turbine installed within the duct which will, in turn, generate electricity [27]. The present paper assessed the geospatial availability of nearshore wave power to target the regions of highest energy generation potential while also reducing environmental impacts associated with larger system sizes [11]. Nearshore OWC point absorbers were the focus of the study, as opposed to offshore OWCs, because these unique systems offer a utility of converting wave power to electricity close to the shoreline where commercial, residential, and industrial electricity demand exists [17]; [33].

The energy generation potential of energy systems, especially renewable energy systems, is highly dependent on the spatial location of that system [11]; [33]. For example, the amount of energy that a solar panel farm will generate is conditional on the insolation and incident solar angle. Likewise, wind farm generation potential depends on boundary layer flows and surface friction. This differential distribution of resources, which fuel renewable energy systems, results in some locations clearly being the optimal installation sites.

In the case of OWCs, ocean environments which naturally generate waves of higher amplitude and period will allow the energy conversion systems to produce higher energy outputs [3]. However, as wave height increases, an OWC system must house a larger chamber volume to accommodate the larger waves heights and ensure that the system functions properly without overflow. This coupled challenge of targeting the shoreline sites of highest energy generation potential while calculating the optimal size of an OWC system at that point is assessed by the algorithm developed in the present paper.

The benefit of advancing renewable energy technologies is in their ability to mitigate global warming potential by having fewer to no greenhouse gas emissions when compared to conventional energy technologies. Although most renewable energy systems have zero emissions during operation, few of these systems can be feasibly manufactured with zero emissions as well. Thus, prompting efforts to reduce emissions during energy system manufacturing as well as during all other life cycle phases. As it was previously established, the spatial location of an OWC system controls its long-term energy output and, in turn, controlling its optimal system size to ensure that energy output can be achieved [11]. Then, as system size varies, the required input material to manufacture the OWC system varies as well. This propagation results in a differential in the environmental life cycle impacts profile of OWCs along the shoreline. The present paper addresses the cost-benefit between establishing locations of highest energy generation potential and designing systems with the lowest greenhouse gas emissions. Such an assessment was conducted through a geospatial life cycle assessment (LCA) in tandem with the algorithm designed to calculate OWC generation potential and system sizes geospatially.

2 Data Retrieval

2.1 Data Sites

To develop this geospatial OWC assessment tool, empirical wave data was obtained from buoy sites in the northeast United States. These data sites are constituents of the Integrated Ocean Observing System (IOOS) and consisted of five buoy stations: A01, B01, E01, F01, I01 [24]. These five buoys, in particular, were selected based on their distance from the shoreline and their data availability. The OWCs assessed in the present paper were nearshore point absorbers, thus, the potential installation sites must be close to the shoreline [5]. The locations of existing buoys limited where the case study assessment could occur; the eastern coastline of New England was preferred as a result of this region having a high density of buoy sites.

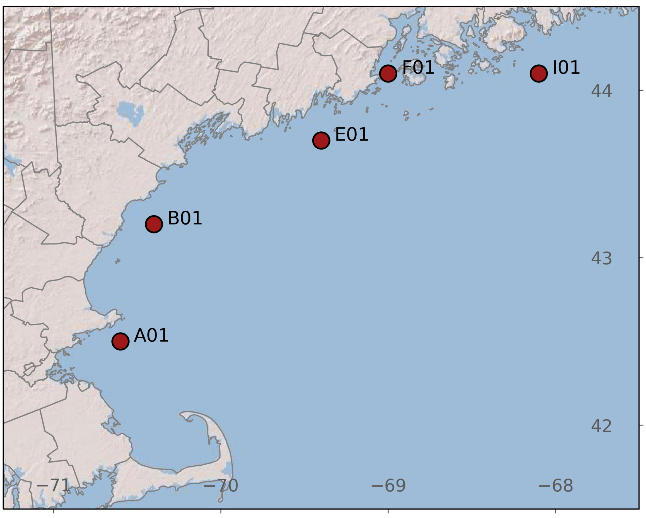

Figure 1: Spatial locations of the five IOOS buoys used for data retrieval in this study. The five buoys included A01, B01, E01, F01, and I01.

Additional IOOS buoys located in this case study region but were excluded from the assessment due to their narrow time frame of archived wave measurements. Buoys A01, B01, E01, F01, and I01 were ideal because they recorded both significant wave height, H_s, and wave period, T, at an hourly temporal resolution over a time frame from 2003 to 2017.

2.2 Data Cleaning

Before the wave height and wave period data could be used in the analysis, missing and erroneously recorded data from the buoy accelerometers had to be removed. The lower temporal limit of the retrieved data for the analysis was 1 January 2003 and the upper limit was 31 December 2017. Within this time frame, each buoy had two sets of approximately 131,400 data points to parse; wave height and wave period. All data points within both the wave period and significant wave height sets are denoted by $\mathbf{t} = (t_{1n}, t_{2n}, t_{3n}, ..., t_{mn})$ where, m is the total number of data points in the respective set and n is the buoy from which that set was retrieved. To clean the missing and erroneous data, each set is parsed by the function $\mathbf{t} > \bar{\mathbf{t}} + 15\sigma$ where, $\bar{\mathbf{t}}$ is the average of the set, $\mathbf{t}$, and σ is the standard deviation of the set. At each data value where the function returned true, that value was nullified. The function's purpose was to control for data that was improperly archived and was not previously marked as missing or erroneous by the IOOS during data collection.

Once all data points were cleaned, they were averaged down from hourly resolution to monthly resolution which reduced the size of each data set from approximately 131,400 points to 180 points while still ranging from 1 January 2003 to 31 December 2017. This procedure was justified by referring back to the scope of the present paper: to 1) design an algorithm that geospatially assesses the energy generation potential of 2) optimally sized OWCs and 3) quantifies the life cycle environmental impacts of system manufacturing. This scope does not require a high temporal resolution of empirical wave data, rather, it is important to have a longer time frame to capture oceanic fluctuation over the lifetime of the OWCs [11]. Reducing the temporal resolution of the data sets to maximize the time frame width aided in reducing computational time.

2.3 Rayleigh Distribution

The five IOOS buoys report wave height as significant wave height; defined as the average of the upper third wave height values of the wave spectrum [1]. The wave spectrum can be well-represented as a Rayleigh distribution with the following probability density function:

$$f(x, \sigma) = \frac{x}{\sigma^2} e^{-\dfrac{x^2}{2\sigma^2}} \qquad (1)$$

where, $x \in [0, \infty)$. σ is a scaling parameter that defines the spread of the distribution [8]; [22].

To obtain the individual wave height value, H_0 , from the given H_s values, the correct σ value must be determined to reconstruct the proper Rayleigh pdf for each wave.

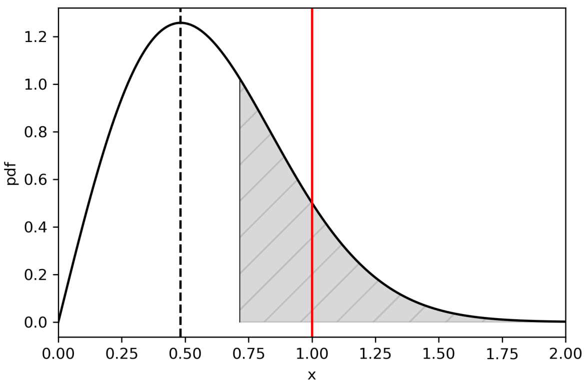

Figure 2: Given $H_s = 1$, the wave spectrum is represented by the Rayleigh distribution with $\sigma = 0.4824$ where the red line denotes H_s, the expected value of the upper third of the wave spectrum. The shaded region marks the upper tercile of the wave spectrum. The dashed black line denotes the individual wave height value, H_0.

A gradient descent method was employed to recover the σ values for a given H_s value. The gradient descent method iteratively solved for σ by reducing the error between a randomly built Rayleigh distribution's upper third expected value and the given H_s value [1]. A random Rayleigh distribution was initialized with $\sigma = 1$ and the expected value was calculated of the upper third of x values. Then, the absolute value of the difference between H_s and the built distribution's upper tercile average until the absolute value of the difference was less than 0.01. If the error was not less than 0.01, then each iteration would add a small $\delta\sigma$ to prior iteration's σ value until the prescribed error threshold was achieved. As the error got smaller, $\delta\sigma$ got smaller to mitigate overshooting the target value. To correct an overshoot, a negatively valued $\delta\sigma$ was added to the prior σ. Once the error threshold was achieved, the gradient descent was run nine more times for each H_s. Until, finally, the average of the ten σ values was used to reconstruct the Rayleigh distribution. H_0 was obtained for each timestep by extracting the median x value of the constructed Rayleigh pdf.

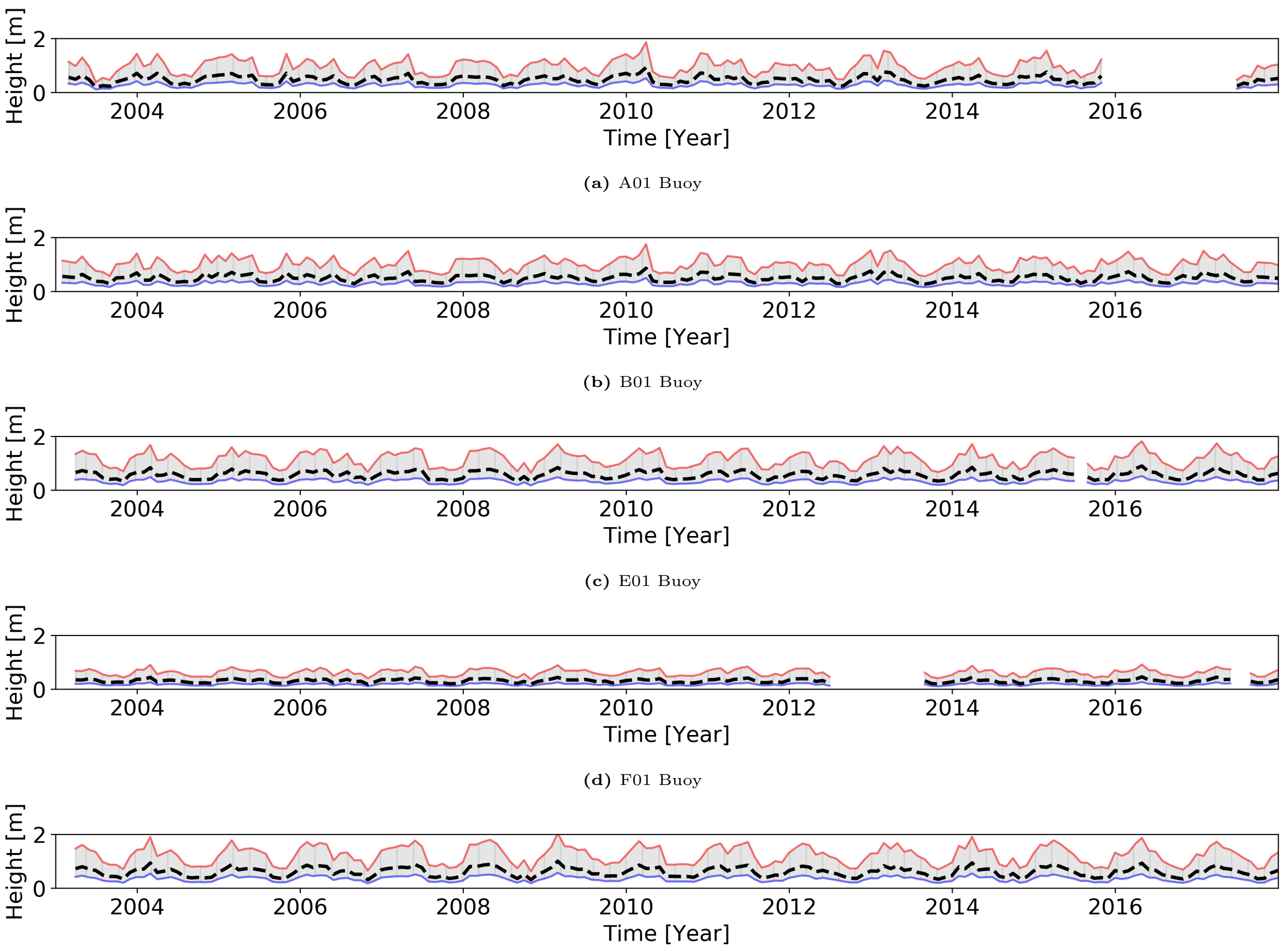

(a) A01 Buoy

(b) B01 Buoy

(c) E01 Buoy

(d) F01 Buoy

(e) I01 Buoy

Figure 3: The calculated individual wave height values recovered using the Rayleigh distribution gradient descent method. The red line corresponds to the significant wave height values, H_s, obtained from the respective buoys. Thus, the red line is also the average of the upper tercile of the wave spectrum. The dashed black line is the median value of the wave spectrum, therefore, it represents the individual wave height, H_0. The blue line is the average of the lower tercile of the wave spectrum, for reference.

Figure 3 illustrates the final H_0 values that were recovered from the H_s values using the Rayleigh distribution and the gradient descent method. Iteratively solving for H_0 resulted in wave power values, calculated in **Section 4**, to be closer to what we would expect to see during OWC operation. This is due to $H_s > H_0$ at each time step, hence, using solely H_s to compute wave power would overestimate the estimated energy generation potential of each system.

3 Shoreline Site Selection

Site selection for developing this analysis tool was restricted to regions with abundant data availability from buoys. The potential shoreline sites that were selected along the eastern coastline of New England were within proximity to the buoys. These site coordinates were obtained via extraction from the vertices of a 500k-resolution shapefile retrieved from the U.S. Census Bureau [7]. 6,775 potential shoreline sites were initially extracted but were then refined to ensure these sites were topographically suitable for OWC installation.

A 3 arcsecond, high-resolution coastal relief map was retrieved from NOAA and overlaid onto the 6,775 extracted sites to determine topographic site suitability [14]. 6,256 sites were successfully mapped to the coastal relief values, leaving 519 sites with missing bathymetric height data. Using the successfully mapped heights, the missing values were linearly interpolated so all 6,775 shoreline sites had corresponding height values [21].

Based on the geometry of both functioning and prototype OWC systems from existing literature, explored in **Section 5.1**, the system chamber requires at least 3.5 m of functioning lip draught height and at least 3.5 m of functioning chamber opening height. The lip draught of the system is the height of material below the water line and above the chamber opening. The chamber opening is the entrance for the working fluid to enter the system chamber. Thus, each of the potential shoreline sites had to be at least 7.0 m below sea level, which corresponds to a bathymetric height of −7.0 m in the coastal relief data set. All 6,775 sites were parsed and only the sites with bathymetric heights less than or equal to −7.0 m would comprise the final set of shoreline sites. After parsing, 1,675 shoreline sites were quantified as suitable for OWC installation.

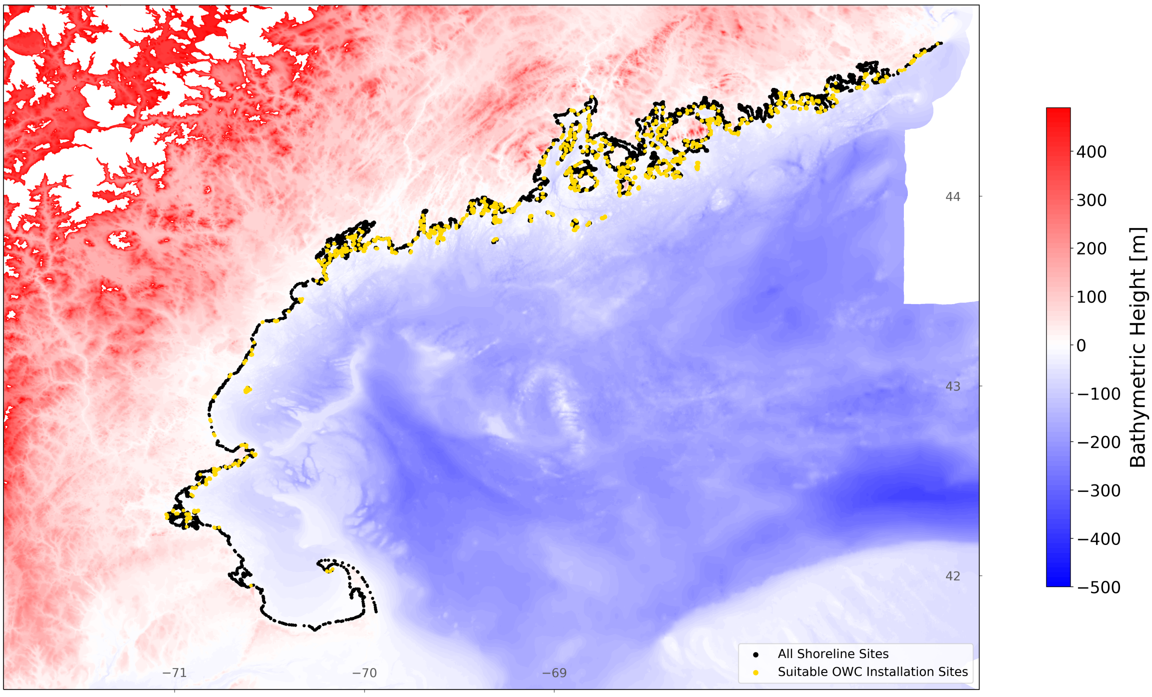

Figure 4: Black points correspond to all 6,775 initial shorelines sites. Yellow points correspond to the suitable shoreline sites where OWC installation was deemed possible. At the suitable shorelines sites, the bathymetry had a height less than or equal to −7.0 m. The colorbar corresponds to the bathymetric data retrieved from the NOAA coastal relief model.

4 Wave Power Algorithms

4.1 Power Equation

With 180 timesteps of wave period and significant wave height from 1 January 2003 to 31 December 2017 at each of the five buoys, wave power values at each of these timesteps were estimated. Estimated wave power is a function of the two empirical variables, wave period, T, and individual wave height, H_0:

$$P(T, H_0, \eta) = \frac{\rho_w g^2 T H_0^2 \eta}{32\pi} \tag{2}$$

where, P is the estimated wave power. $\rho_w = 1,025\,\mathrm{kg\,m^{-2}}$ is the density of sea water, treated as a constant. $g = 9.81\,\mathrm{m\,s^{-2}}$ is the gravitational acceleration. η is the efficiency of the Wells turbine installed in the OWC chamber duct [5]; [6]; [23]; [30]; [33].

At every timestep, this power equation iterated over the wave height and period values for all five buoys, resulting in five temporal matrices being constructed.

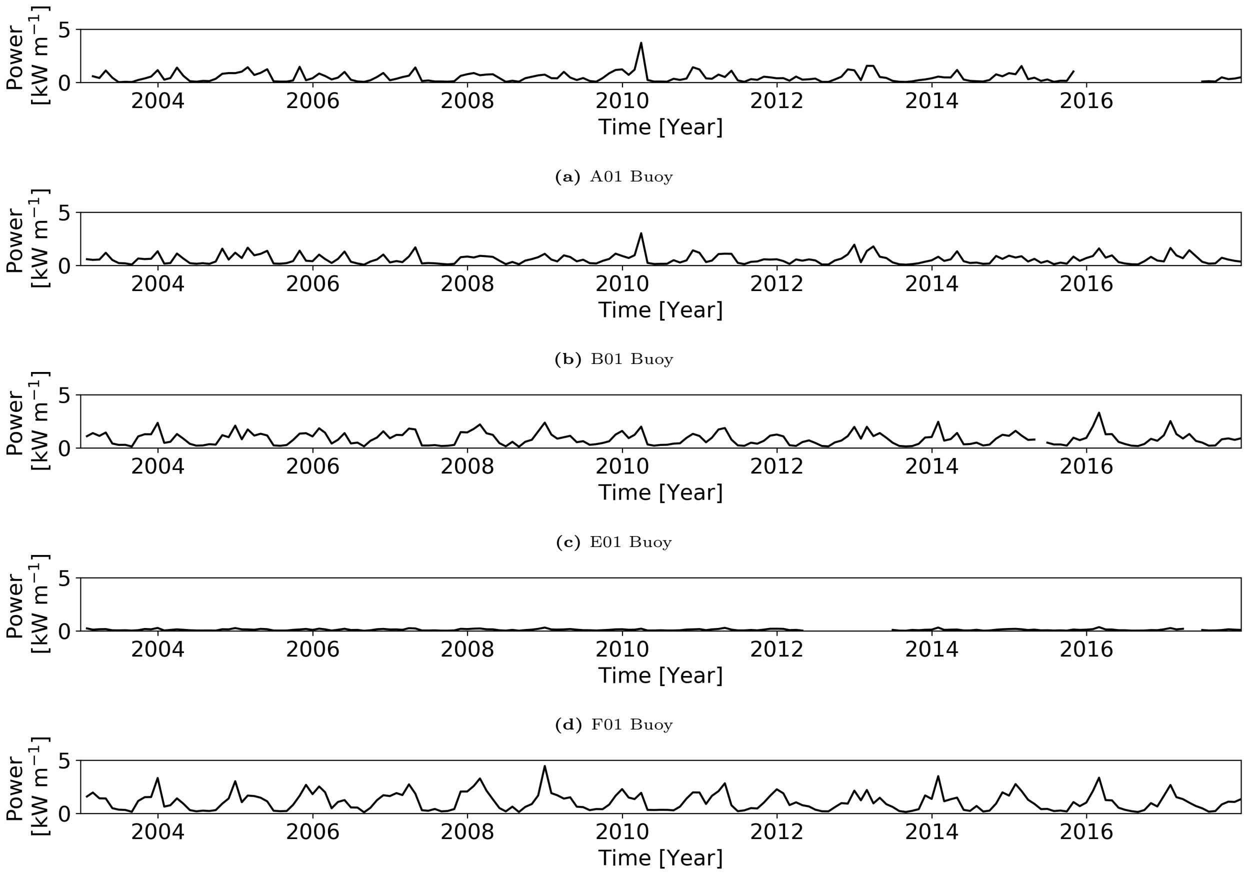

(a) A01 Buoy

(b) B01 Buoy

(c) E01 Buoy

(d) F01 Buoy

(e) I01 Buoy

Figure 5: A visualization of the five calculated wave power temporal matrices at each IOOS buoy using equation (2).

4.2 Geospatial Estimation

To estimate the nearshore wave power, these five matrices, spatially represented as point data, of average monthly wave power were translated into a meshgrid. Through this geometric translation, the variability of wave power values begins to be captured geospatially [19]. The meshgrid was built with longitude and latitude bounds of $x \in [-70.617, -69.938]$, $y \in [41.810, 42.977]$, respectively, and a grid resolution of 100 x 100. These bounds were subsampled from the furthest extending shoreline sites assessed in the study to ensure all sites were enclosed withing the meshgrid bounds. The x- and y-values of the meshgrid bounded the longitude and latitude of the frame whereas the z-values of the meshgrid were given by the estimated power values. The meshgrid was initialized at every time step by setting five out of the 1,000 grid z-values equal to the five wave power matrices at the buoy coordinates on the meshgrid. The remaining grid points that did not correspond to buoys coordinates were interpolated by the following radial Gaussian decay function:

$$z_f(x_i, x_f, y_i, y_f, z_i) = z_i e^{-\left(\frac{\sqrt{(x_f - x_i)^2 + (y_f - y_i)^2}}{\epsilon}\right)^2} \tag{3}$$

where, z_f is the interpolated z-value at the target longitude and latitude values, x_f and y_f. x_i and y_i are the longitude and latitude values corresponding to the locations of the initialized z-values at the five buoy locations; $i \neq f$. z_i is one of the five initialized power values estimated at the buoy locations. ϵ is a constant parameter that approximates the average distance between all five initialized buoy locations; as $\epsilon \to \infty$, $z_f \to z_i$ [21].

4.3 Shoreline Site Wave Power Mapping

The initialized meshgrid was iterated 180 times, once for every timestep, using (3) to obtain an interpolated wave power value at every grid point. Using the coordinates of all 1,675 suitable shoreline sites, each iteration subsampled the respective interpolated power value from the meshgrid. Then, all power values were compiled into a matrix with their corresponding longitude and latitude values:

$$\mathbf{A_{i\times j}} = \begin{bmatrix} x_1 & y_1 & z_{f_{11}} & z_{f_{12}} & \cdots & z_{f_{1j}} \\ x_2 & y_2 & z_{f_{21}} & z_{f_{22}} & \cdots & z_{f_{2j}} \\ \vdots & \vdots & \vdots & \vdots & \ddots & \vdots \\ x_i & y_i & z_{f_{i1}} & z_{f_{i2}} & \cdots & z_{f_{ij}} \end{bmatrix} \tag{4}$$

where, **A** is the temporal matrix of subsampled shoreline site wave power values. $i = 1,675$ is the number of suitable shoreline sites. $j = 180$ is the number of timesteps. x, y are longitude, latitude. z_f are the interpolated wave power values at the corresponding (x, y) coordinates.

By collapsing the columns of wave power values, all timesteps were averaged together and the 0.1-trimmed mean was calculated:

$$\mathbf{B_{i\times 3}} = \begin{bmatrix} x_1 & y_1 & z_{t_1} \\ x_2 & y_2 & z_{t_2} \\ \vdots & \vdots & \vdots \\ x_i & y_i & z_{t_i} \end{bmatrix} \tag{5}$$

where, **B** is the time-averaged matrix of power values at all suitable shoreline sites. z_t are the 0.1-trimmed average wave power values at the corresponding (x, y) coordinates.

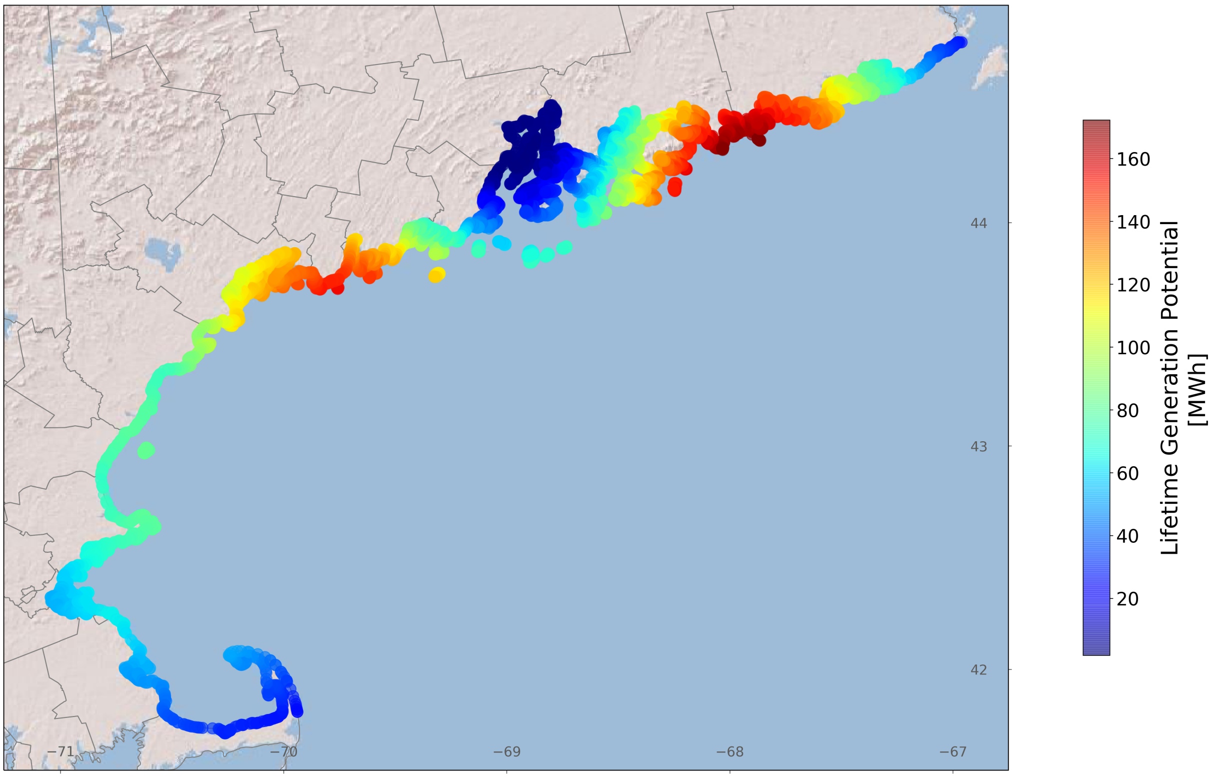

(a)

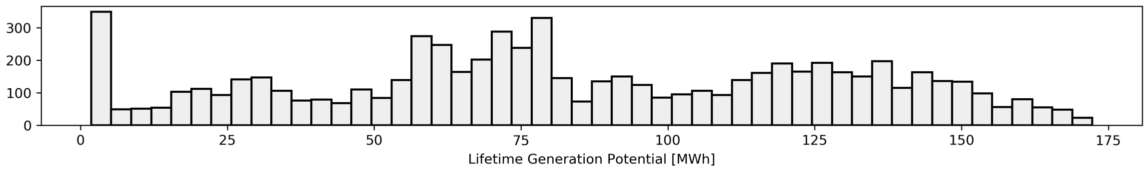

(b)

Figure 6: (6a) Geospatial energy generation potential across the entire case study shoreline, $i = 6,775$. The lifetime of an OWC system is estimated to be 20 years [11]. Thus, to obtain the generation potential over the lifetime of the system, the hourly system energy is multiplied by the number of hours in 20 years. (6b) Histogram of lifetime energy generation potential values along the shoreline, $N = 6,775$.

Wave power values were estimated temporally first before averaging down to a single value for each site to reduce error and gain a more accurate representation of the ocean conditions. The importance of taking the average of the power estimations is in the optimization of the OWC chamber size; a chamber will be optimally sized when the chamber size becomes a function of the system's most typical value of power over its lifetime. A 0.1-trimmed mean of 15 years of wave power values captures this typical wave power value over the system's lifetime by representing the temporal set and removing outliers.

The steepest gradient in lifetime energy potential values occurs at the opening of the Casco Bay (-68.7° longitude) with a maximum of 172.3 MWh and a minimum of 1.8 MWh. The energy potential of an OWC is highly dependent on the oceanic conditions and the shoreline structure, implying that the siting of the system plays a role in its potential to generate electricity [33]; [11]. The steep gradients in lifetime energy potential values revealed in **Figure 6** illustrate the importance of conducting geospatial energy analyses for renewable energy systems due to the variability in energy values along a short length of coastline. Without first targeting the locations of highest energy potential, an installed system may end up having significantly higher costs than benefits even when the system sizes are scaled proportional to the estimated energy potential [11]. In the present paper, the costs of system installation were quantified by life cycle environmental impacts in **Section 6**.

5 System Engineering

5.1 OWC Chamber Geometry

To size each shoreline OWC system based on its estimated generation potential, the system geometry must be studied. For this study, a simple rectangular chamber design was used to model the system geometry as shown below.

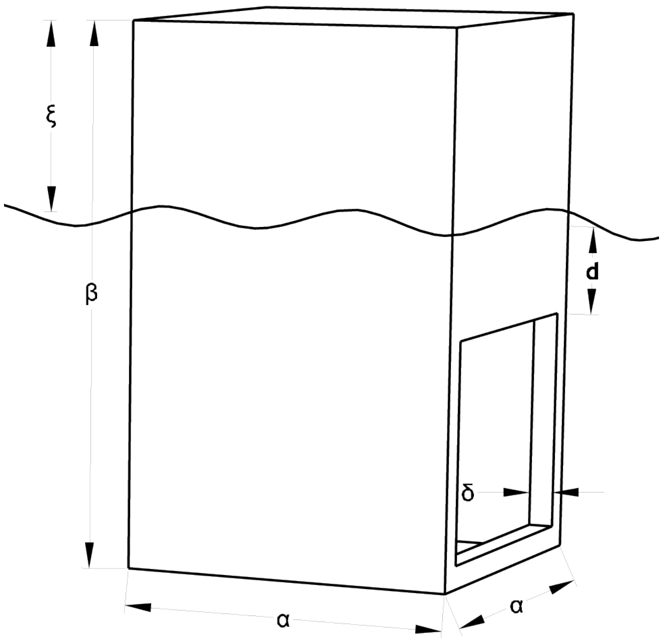

Figure 7: A sketch of the OWC chamber geometry where, α^2 is the chamber cross-sectional area. β is the total chamber height. ξ is the chamber height above the water. δ is the chamber wall thickness. d is the lip draught height.

From the five geometric components of the chamber, α^2, β, ξ, δ, and d, each system could be optimally sized for its environmental boundary conditions. The cross-sectional area component was calculated using the estimated generation potential. The total chamber height is a function of bathymetric height at the site coordinates, $\tau(x, y)$, and ξ. The ξ, δ, and d components were controlled as constants from existing literature values.

From existing literature on OWC chamber geometry, it is noted that a wide distribution of chamber geometries exists. The most variable geometric component is chamber cross-sectional area, α^2. By strictly calculating this value through the later developed optimization process in **Section 5.2** rather than treating it is a constant, significant error is avoided. With cross-sectional area having the highest value range of $320\,\mathrm{m}^2$, the values from existing literature were, $\alpha^2 : \{4\,\mathrm{m}^2, 30\,\mathrm{m}^2, 64\,\mathrm{m}^2, \sim 87.5\,\mathrm{m}^2, 324\,\mathrm{m}^2\}$ [3]; [5]; [13]; [29]. Some of these values were retrieved from model-to-prototype ratio scales while others were retrieved from functioning OWCs that were once in operation. The distribution of these values from different OWCs illustrates the impact that the difference in oceanic conditions has on the scaling of a system while still allowing it to function [33].

Total chamber height, β, was calculated as summation of bathymetric height, $\tau(x, y)$, and chamber height above water, ξ. Chamber height above water is the first constant geometric component. This value has the second highest range of 17.5 m, the values from existing literature were, $\xi : \{7.5\,\mathrm{m}, 10.8\,\mathrm{m}, \sim 13\,\mathrm{m}, 25\,\mathrm{m}\}$ [3]; [5]; [13]; [29]. The sea level was kept as a constant during this assessment and was quantified by $\tau(x, y) = 0$. The value of ξ is necessary because a volume of air must be left above the working fluid such that the compression and expansion of air within the chamber will allow for an airflow across the turbine, which is installed above $\tau(x, y) = 0$ [6]. An approximate median value of ξ was retrieved from literature resulting in $\xi = 12\,\mathrm{m}$.

The constant variable with the next highest range is the lip draught height. This lip is necessary to keep the air within the system and only interacting with the environment through the duct where the turbine exists. If the water level falls below the lip draught, then the internal pressure will equalize with the surrounding environment, breaking down the system dynamics and diminshing system efficiency [6]; [30]. The lip is also an important factor in the efficiency of the OWC [3]. From literature, the lip draught height has a range of 5.6 m, with a distribution of $d : \{1.9\,\mathrm{m}, \sim 3\,\mathrm{m}, 3.6\,\mathrm{m}, 7.5\,\mathrm{m}\}$ [3]; [5]; [13]; [29]. An approximate median value was retrieved as $d = 3.5m$.

The final constant variable is the chamber wall thickness, δ. δ also estimates the height below the chamber opening and the width to each side of the chamber opening. δ has a range of 0.48 m with a tight distribution of values from literature, $\delta : \{0.12\,\mathrm{m}, 0.5\,\mathrm{m}, 0.6\,\mathrm{m}\}$ [3]; [5]; [13]; [29]. Thus, an approximate median value was retrieved as $\delta = 0.35\,\mathrm{m}$.

5.2 Optimization Algorithm

As established, the cross-sectional area, α^2, is the geometric component of the OWC chamber that will be sized as a function of the wave power estimations at each shoreline site. Through application of this algorithm to the data, the internal volume of the chamber can be calculated to best fit its oceanic conditions [18]. The 15-year 0.1 trimmed mean of wave power at each site provides a good estimation of the general conditions these systems will experience during their lifetime. By scaling the system sizes to meet the supplied power of the waves at that location, excess material is not wasted by making the chamber too large and the maximum possible generation is achieved because the system is not too small.

To assess α^2 as a function of supplied wave power, the appropriate algorithm must be developed. The first set of governing equations are associated with relating wave power to horsepower then horsepower to air velocity over the turbine:

$$\underline{P} = PH_0 \times 1.34102 \tag{6}$$

$$\underline{P} = \frac{V_x A_d P_a}{6356} \tag{7}$$

where, $\underline{P}$ is wave power in horsepower. P is the estimated wave power from (2). H_0 is the individual wave height. V_x is the velocity of air over the turbine in the chamber. A_d is the cross-sectional area of the duct where the turbine is installed. P_a is the air pressure within the turbine duct [15].

V_x is currently an unknown value, however, we have values of P, H_0, and A_d. Also, P_a is a value retrieved from experimental studies of OWC chamber dynamics. We pick the maximum observed value of $P_a = 7000\,\mathrm{Pa}$ to be the estimated air pressure within the turbine duct [23]. Rearranging (7) to solve for V_x allows the chamber cross-sectional area to be calculated by the following governing equation:

$$\alpha^2 = \frac{V_x A_d}{\left(\frac{\delta H_0}{\delta t}\right)} \tag{8}$$

where, α^2 is the cross-sectional chamber area. $\frac{\delta H_0}{\delta t}$ is the change of the water column height over time within the chamber [28].

Applying Leibniz's integration rule [16] and the fact that wave height is a function of time, $H_0(t)$, we have:

$$\frac{\delta H_0}{\delta t} \approx \frac{\delta}{\delta t}\left(\int_{t_0}^{t_1} H_s(t)dt\right). \tag{9}$$

Since, the bound width is constant for each timestep,

$$\frac{\delta}{\delta t}\left(\int_{t_0}^{t_1} H_0(t)dt\right) = \int_{t_0}^{t_1} \frac{\delta H_0(t)}{\delta t}dt \approx \int_{t_0}^{t_1} dH_0. \tag{10}$$

Applying the Fundamental Theorem of Calculus, we get:

$$\int_{t_0}^{t_1} dH_0 = H_0(t_1) - H_0(t_0) = \Delta H_0. \tag{11}$$

Thus, we approximate:

$$\frac{\delta H_0}{\delta t} \approx \Delta H_0. \tag{12}$$

Therefore, we may estimate the chamber cross-sectional area using our initial temporal matrix of individual wave height values such that:

$$\alpha^2 = \frac{V_x A_d}{\Delta H_0(t)}. \tag{13}$$

Finally, combining (6), (7), and (13) builds the algorithm that links chamber size to estimated wave power:

$$\alpha^2 = \frac{PH_0(t_0) \times 6356 \times 1.34012}{P_a \Delta H_0(t_0, t)} \tag{14}$$

in which all variables are known or were previously calculated [29]. By applying this algorithm, each estimated wave power value has an optimized chamber cross-sectional area value at every shoreline site. These α^2 values, in combination with the remaining geometric components of **Figure 7**, allow for the calculation of system material consumption at each site.

5.3 OWC Material Consumption

Calculating the volume of concrete material consumed by each OWC system at their respective shoreline sites builds a cost-benefit for system installation. Such that larger OWC chambers with the potential to generate more energy over their lifetimes will consume more material to manufacture and, in turn, have higher environmental impacts prior to normalization by the functional unit [11]; [31].

Referencing **Figure 7**, the following represents the total volume of chamber material without a chamber opening:

$$(2\alpha^2 + 4\alpha\beta)\delta \tag{15}$$

and the chamber opening is represented by:

$$(x - 2\delta)(\tau(x, y) - d - \delta)\delta \tag{16}$$

thus, by combining (15) and (16), we get an equation for the total material consumed by the chamber:

$$(2\alpha^2\delta) + (3\alpha\beta\delta) + ([d + \xi]\delta). \tag{17}$$

A chamber opening for the turbine duct is neglected in (17) because its geometry was kept constant for all systems in this analysis. Applying (17) to the chamber cross-sectional area optimization algorithm in (14) results in the building of a chamber concrete consumption profile along the coastline.

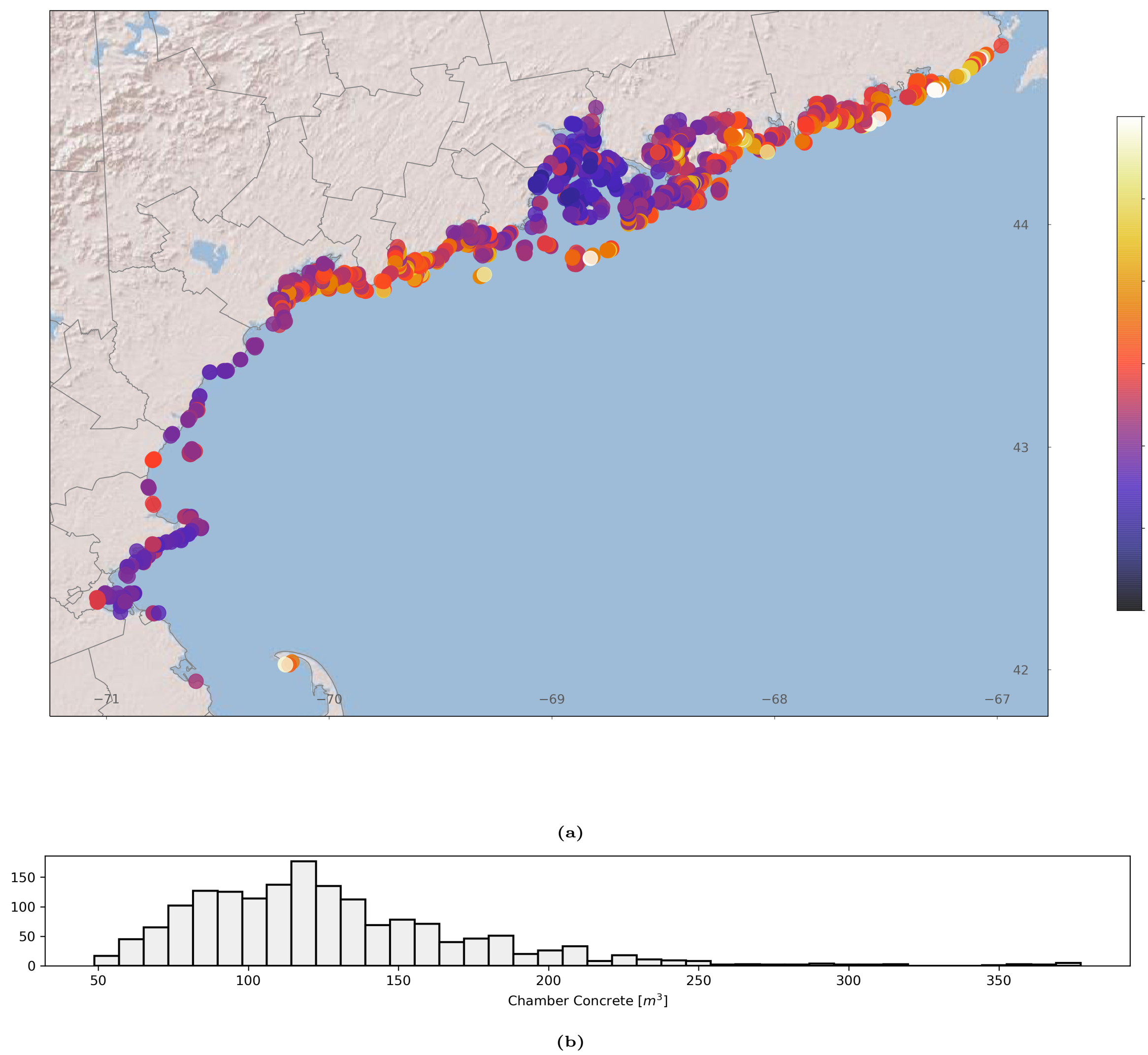

Figure 8: (8a) The geospatial concrete consumption as calculated by (14) and (17). (8b) Histogram of concrete consumption along the shoreline, $N = 1,675$.

Each of these chamber concrete values have been sized proportional to the estimated wave power available at each site using (14). Since the concrete consumption is a function of wave power, it can be noted that where we see the lowest values concrete usage correspond to the lowest values of wave power in the Casco Bay, illustrated by **Figure 6**. The steep gradient of values at the opening of the Casco Bay in **Figure 8** is resolved similarly to the gradient of wave power seen in **Figure 6** at the Casco Bay. Additionally, there are extreme values of chamber concrete which transpire from not limiting the suitable shoreline sites with an upper limit of bathymetric height. The suitable sites had to be at least 7 m below sea level to install a functioning OWC, there was no limit to how deep these sites could be, resulting in unrealistic OWC chamber heights at some locations. These sites were not removed because it is not impossible to install a functioning OWC system there, only impractical.

6 Life Cycle Impacts

6.1 Assessment Type

To quantify the costs, i.e. the environmental impacts, of each OWC system along the New England shoreline, a cradle-to-grave life cycle assessment (LCA) is conducted for each system. This type of assessment will factor in all of the resources consumed and their associated emissions or impacts in the manufacturing, transportation, and disposal phases over the 20-year lifetime of the OWC [11]. The emissions included in this cradle-to-grave LCA were only those associated with climate change impacts. Therefore, all emissions that invoke an atmospheric warming effect were equated to a carbon dioxide equivalent based on said emission's magnitude of warming. Hence, the quantifying units of the LCA were kg of carbon dioxide equivalent.

Each system's impacts were then normalized by their lifetime energy generation potential in kWh, allowing the impact magnitude to be compared on a system-to-system basis. For example, if two OWC systems are compared and each require the same input of material but one system generates significantly more energy over its lifetime, then the higher energy producer system will have lower impacts for every kWh of functionality. Therefore, we denote kWh as our functional unit in the LCA [31].

6.2 Assessment Components

The first component of the LCA is the climate change impact of concrete production. The magnitude of impact is obtained from the Ecoinvent database where one cubic meter of concrete, made with cement type CEM II/B, has a life cycle impact (LCI) on climate change of $172.6\,\mathrm{kg\,CO_2\,eq/m^3}$ [4]. This Ecoinvent impact assessment was calculated using TRACI 2.1 V1.03/US 2008. Concrete made with CEM II/B was selected over CEM II/A and CEM I due to it having a lower clinker concentration which decreases the grain size and permeability of the structure; CEM III LCIs were not available from the database [2]; [26]. To get the total impact of concrete production for each OWC system along the shoreline, the LCI was multiplied by the required amount of concrete to manufacture each system, shown in **Figure 8**, and then normalized by lifetime energy potential, shown in **Figure 6**.

The next component is the LCI of the turbine and generator for each OWC. The turbine and generator set has an LCI of $0.344\,\mathrm{kg\,CO_2\,eq/set}$ calculated using TRACI 2.1 V1.03/US 2008 [4]. Each OWC system only has one turbine and generator resulting in a lower climate change impact compared to that of the concrete production. The turbine and generator LCI was also normalized by lifetime energy potential, shown in **Figure 6**.

The final component of the LCA is the LCI of product transportation to the deployment site. The concrete must be transported from the point where it was mined or refined to the coastline site where it is poured to shape the OWC chamber. Concrete is comprised primarily of silica compounds so the point used as a production site of the concrete was largest producer of silica in the northeast - a mine located in northwest New Hampshire [32].

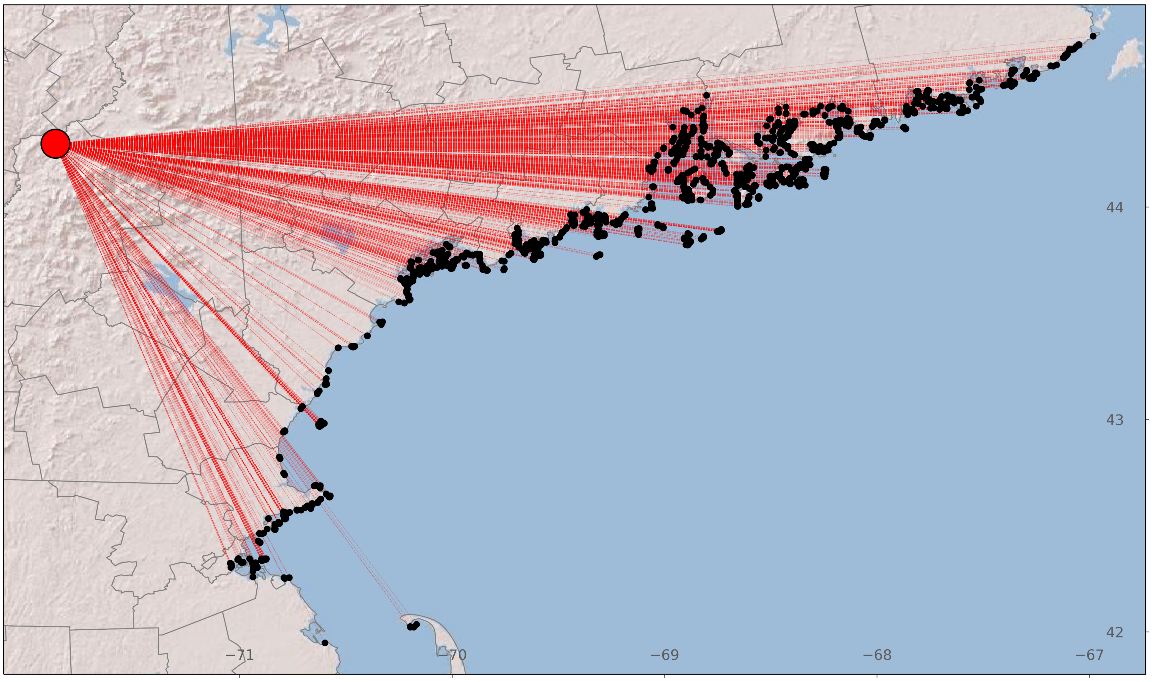

Figure 9: The red point marks the silica production site in northwest New Hampshire. The black points are the OWC deployment sites along the shoreline. The dashed red lines indicate the shortest distance between the silica production site and the OWC deployment sites.

The distances obtained between the silica production site and the OWC deployment sites represent the shortest possible distances to transport the concrete. Therefore, an additional distance of 20% is added to each transportation route to get a better estimate of the distance that a freight train must travel to reach each individual site. The LCI of a diesel-powered train is $2.20 \times 10^{-5}\,\mathrm{kg\,CO_2\,eq/kg \cdot m}$ which was calculated using TRACI 2.1 V1.03/US 2008 [4]. The distance traveled from **Figure 9** and the mass of the concrete being transported, obtained using a CEM II/B density of $2,800\,\mathrm{kg/m^3}$, were multiplied by the LCI then normalized by the lifetime energy potential, shown in **Figure 6** [26].

The summation of the total impacts of concrete production, turbine and generator production, and material transportation quantifies the total lifetime impact for each OWC system. Iterating this analysis across all shoreline sites builds a profile for OWC LCIs along the coast, shown in **Figure 10**.

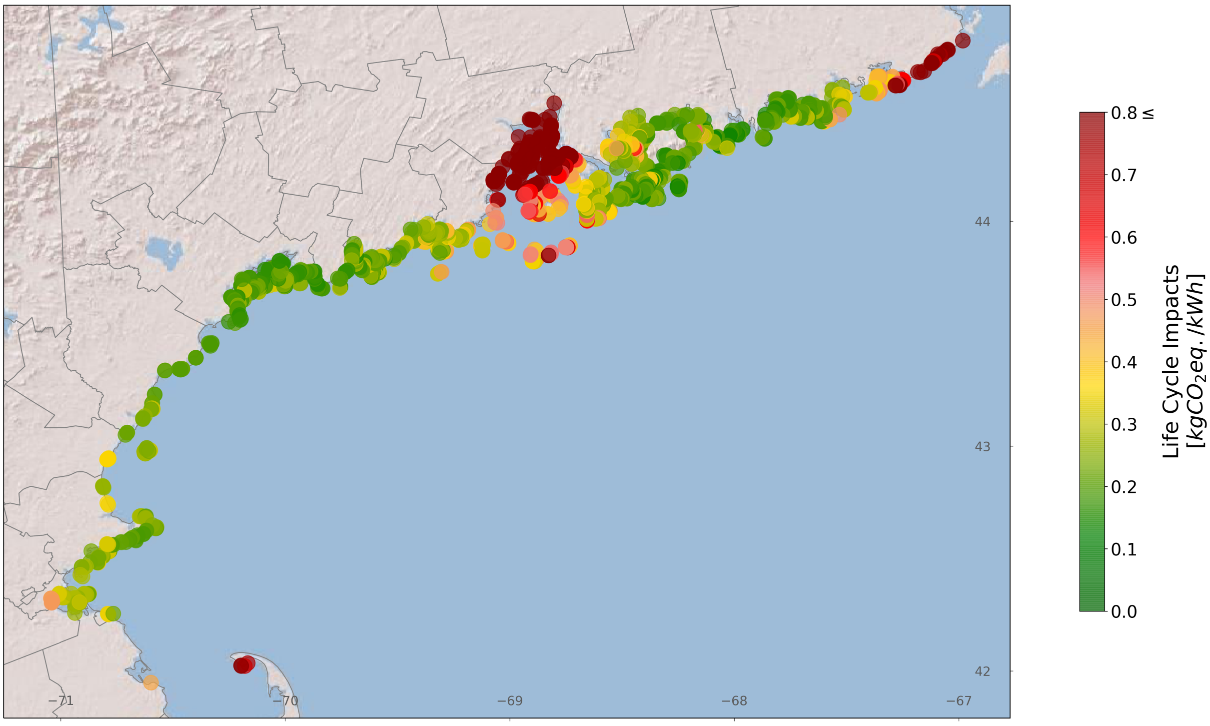

(a)

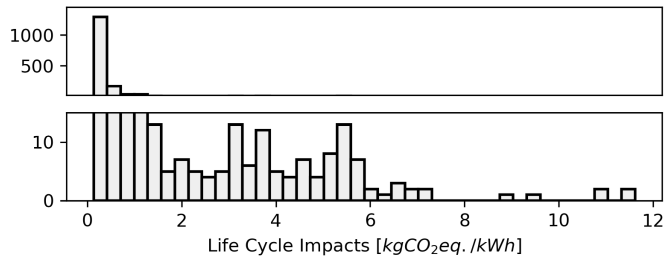

(b)

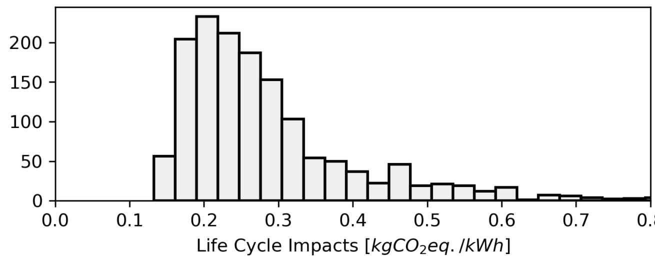

(c)

Figure 10: (10a) Geospatial life cycle environmental impacts for each optimally sized OWC system at its deployment site. (10b) Histogram of life cycle impacts along the shoreline with y-axis break, $N = 1,675$. (10c) A magnified view the 0 kg CO_2 eq/kWh to 0.8 kg CO_2 eq/kWh x-axis section of the histogram from (10b) with an increased bin number.

Figure 10 illustrates the geographic dependence of OWC LCIs along the New England coastline. The majority of systems along the coastline had LCIs between 0.10 kg CO_2 eq/kWh and 0.35 kg CO_2 eq/kWh. These low LCI values correspond to the regions of high generation potential in **Figure 6**. Even though, by **Section 5.2**, the optimal chamber size is scaled proportional to wave power which, in turn, results in a higher concrete consumption, these locations along the coastline still have the lowest impact per kWh.

The regions of highest LCI correspond closer to regions of lower energy potential rather than regions of higher concrete consumption. Many of the outliers seen in **Figure (10b)** have a frequency less than 20 and are primarily seen where the lifetime generation potential is less than 40 MWh. As shown in **Figure 8**, concrete consumption is not necessarily highest in these regions of high LCI; the sites deep within the Casco Bay illustrate this. Most Casco Bay systems require less than 100 m^3 of concrete for chamber manufacturing, yet have exceedingly high emissions per kWh. Due to the low lifetime generation potential within the bay, every kWh generated by an OWC there has a higher cost, i.e. environmental impact, as a result of less energy being generated at these sites.

With the highest frequency LCI values falling within the range of 0.10 kg CO_2 eq/kWh to 0.35 kg CO_2 eq/kWh, as shown in **Figure (10c)**, most renewable energy system LCIs fall below this range whereas conventional energy LCIs fall above this range. Silicon photovolatics have a baseline LCI of 0.045 kg CO_2 eq/kWh, wind turbines have a baseline LCI of 0.011 kg CO_2 eq/kWh, hydropower systems have a baseline LCI of 0.0040 kg CO_2 eq/kWh, natural gas plants have a baseline LCI of 0.47 kg CO_2 eq/kWh, and coal-fired power plants have a baseline LCI of 0.98 kg CO_2 eq/kWh [20]; [10]; [12]; [25]; [34]. Therefore, indicating that most OWCs installed along this coastline do not have the potential to be as sustainable as other more common renewable energy systems. However, they are, in fact, more sustainable than conventional methods of energy generation. To ensure that these OWC are at least more sustainable than conventional energy systems, the location of the installation site is paramount. Poor selection of an installation site may result in LCIs higher than those of coal or natural gas power plants.

7 Conclusion and Discussion

In this study, it was determined that geographic positioning of an OWC installation site has influence on the OWC's lifetime energy generation potential and life cycle impacts on climate change. Shifting the installation site of an OWC along the shoreline resulted in significant changes in LCI which could make that OWC system less sustainable or more sustainable than conventional energy systems, such as coal or natural gas.

It was found that the sustainability profile of OWC installation along the shoreline, quantified by LCI, followed a similar spatial evolution as the lifetime energy generation potential profile. By developing an algorithm that optimally sized an OWC chamber to its oceanic boundary conditions, system size and, in turn, concrete consumption were also dependent on the geographic location of an OWC installation site. However, this variation in concrete consumption along the shoreline was less representative of LCIs than the energy generation along the shoreline.

Steep gradients of LCI values were seen in regions of complex shoreline structure, notably in the Casco Bay where energy generation potential is at a minimum. Significant changes in both LCI and generation potential along this particular coastline of New England emphasize the importance of proper planning and analysis prior to installing or manufacturing OWCs. Since the effectiveness of a renewable energy system, OWCs in this case, is highly dependent on the system's surrounding environment, a careful exploration of the energy potential and life cycle impact profiles of the surrounding environment should be conducted to ensure the system meets its highest output and lowest impact.

In future work, a more refined analysis of coastal and nearshore topography will be conducted to study the influences of coastal geometry on the wave power harvestable by ocean energy systems [6]; [9].

References

[1] U.S. Naval Academy. *Rayleigh Probability Distribution Applied to Random Wave Heights*. n.d.

[2] F. Arena et al. "On Design and Building of a U-OWC Wave Energy Converter in the Mediterranean Sea: A Case Study". In: *Proceedings of the ASME 2013 32nd International Conference on Ocean, Offshore and Arctic Engineering* (2013), pp. 1 –8.

[3] S. John Ashlin, S.A. Sannasiraj, and V. Sundar. "Wave Forces on an Oscillating Water Column Device". In: *Procedia Engineering* 116 (2015). 8th International Conference on Asian and Pacific Coasts (APAC 2015), pp. 1019 –1026.

[4] J.C. Bare. "TRACI 2.0 - The Tool for the Reduction and Assessment of Chemical and other environmental Impacts". In: *Clean Technologies and Environmental Policy* 13.5 (2011), pp. 687–696.

[5] H.B. Bingham et al. "Hydrodynamic analysis of oscillating water column wave energy devices". In: *Journal of Ocean Engineering and Marine Energy* 1.4 (2015), pp. 405–419.

[6] B. Bouali and S. Larbi. "Contribution to the Geometry Optimization of an Oscillating Water Column Wave Energy Converter". In: *Energy Procedia* 36 (2013). TerraGreen 13 International Conference 2013 - Advancements in Renewable Energy and Clean Environment, pp. 565 –573.

[7] U.S. Census Bureau. *Geography: Cartographic Boundary Files.* 2017.

[8] D.E. Cartwright and M.S. Longuet-Higgins. "The Statistical Distribution of the Maxima of a Random Function". In: *Proceedings of the Royal Society of London. Series A, Mathematical and Physical Sciences* 237.1209 (1956), pp. 212–232.

[9] J. Davidson, S. Giorgi, and J.V. Ringwood. "Linear parametric hydrodynamic models for ocean wave energy converters identified from numerical wave tank experiments". In: *Ocean Engineering* 103 (2015), pp. 31 –39.

[10] S.L. Dolan and G.A. Heath. "Life Cycle Greenhouse Gas Emissions of Utility-Scale Wind Power". In: *Journal of Industrial Ecology* 16 (2012), pp. 136–154.

[11] S. Draycott et al. "Assessing the Macro-Economic Benefit of Installing a Farm of Oscillating Water Columns in Scotland and Portugal." In: *Energies* 11.10 (n.d.).

[12] O. Edenhofer et al. "IPCC special report on renewable energy sources and climate change mitigation". In: *Renewable Energy Sources and Climate Change Mitigation. Contribution of Working Group III of the Intergovernmental Panel on Climate Change.* Cambridge, United Kingdom and New York, NY, USA: Cambridge University Press, 2011.

[13] A. Elhanafi et al. "Experimental and numerical measurements of wave forces on a 3D offshore stationary OWC wave energy converter". In: *Ocean Engineering* 144 (2017), pp. 98 –117.

[14] NOAA: National Centers for Environmental Information. *NCEI U.S. Coastal Relief Model: Vol. 1 - Northeast Atlantic.* 1998.

[15] E.J. Finnemore and J.B. Franzini. In: *Fluid Mechanics with Engineering Applications, Tenth edition.* McGraw-Hill, 2002.

[16] P. Haile. *Yale Economics: Differentiating an Integral.* 2018.

[17] T.V. Heath. "A review of oscillating water columns." In: *Philosophical Transactions of the Royal Society London, Series A (Mathematical, Physical and Engineering Sciences)* 370.1959 (2012), pp. 235 –245.

[18] J.C.C. Henriques et al. "Design of oscillating-water-column wave energy converters with an application to self-powered sensor buoys". In: *Energy* 112 (2016), pp. 852 –867.

[19] Y. Hisaki. "Time interpolation of stationary and propagating surface disturbances for ocean modeling." In: *Earth and Space Science* 3.9 (2016), pp. 346 –361.

[20] D. D. Hsu et al. "Life Cycle Greenhouse Gas Emissions of Crystalline Silicon Photovoltaic Electricity Generation". In: *Journal of Industrial Ecology* 16 (2012), pp. 122–135.

[21] E. Jones, T. Oliphant, P. Peterson, et al. *SciPy: Open source scientific tools for Python.* 2001–.

[22] G. Maymon. "Chapter 2 - Some Important Statistical Distributions". In: *Stochastic Crack Propagation.* Ed. by G. Maymon. Academic Press, 2018, pp. 9 –18.

[23] S.K. Mishra, S. Purwar, and N. Kishor. "Maximizing Output Power in Oscillating Water Column Wave Power Plants: An Optimization Based MPPT Algorithm." In: *Technologies* 6.1 (2018), p. 15.

[24] NOAA. *U.S. Integrated Ocean Observing System: Northeast Atlantic (NERACOOS).* 2003–.

[25] P. R. O'Donoughue et al. "Life Cycle Greenhouse Gas Emissions of Electricity Generated from Conventionally Produced Natural Gas". In: *Journal of Industrial Ecology* 18.1 (2014), pp. 125–144.

[26] Cementownia Odra. *Portland-Composite Cement CEM II/B-M (V-LL) 32,5 R.*

[27] S. Raghunathan. "The wells air turbine for wave energy conversion". In: *Progress in Aerospace Sciences* 31.4 (1995), pp. 335 –386.

[28] D. Ramirez et al. "Emulation of an OWC Ocean Energy Plant With PMSG and Irregular Wave Model." In: *IEEE Transactions on Sustainable Energy* 6.4 (2015), pp. 1515 – 1523.

[29] M. Takao and T. Setoguchi. “Air Turbines for Wave Energy Conversion.” In: *International Journal of Rotating Machinery* (2012), pp. 1 –10.

[30] F.R. Torres, P.R.F. Teixeira, and E. Didier. “A methodology to determine the optimal size of a wells turbine in an oscillating water column device by using coupled hydro-aerodynamic models”. In: *Renewable Energy* 121 (2018), pp. 9 –18.

[31] A. Uihlein. “Life cycle assessment of ocean energy technologies”. In: *The International Journal of Life Cycle Assessment* 21.10 (2016), pp. 1425–1437.

[32] USGS. *National Minerals Information Center: Refractory, Abrasive, and Other Industrial Minerals Operations.* 2010.

[33] L. Wang, J. Isberg, and E. Tedeschi. “Review of control strategies for wave energy conversion systems and their validation: the wave-to-wire approach”. In: *Renewable and Sustainable Energy Reviews* 81 (2018), pp. 366 –379.

[34] M. Whitaker et al. “Life Cycle Greenhouse Gas Emissions of Coal-Fired Electricity Generation”. In: *Journal of Industrial Ecology* 16 (2012), pp. 53–72.